NUMERICAL SIMULATIONS OF THE FLOW AROUND A FINITE-HEIGHT CIRCULAR CYLINDER UNDER TURBULENT

by

Yuxiang YING, Tongxiao JIANG, and Deming NIE*

Institute of Fluid Mechanics, China Jiliang University, Hanghzou, China

Original scientific paper
https://doi.org/10.2298/TSCI23S1173Y

To investigate the 3-D characteristics of the flow around a finite-height circular cylinder, this study was based on the CFD technology. The flow was numerically simulated between Re = 1000 and 10000 using the large eddy simulation method to verify and analyze the results. Comparing the instantaneous contours of vorticity for different heights at the same Reynolds number, it can be seen that the free end influences vortex shedding. The instantaneous contours of vorticity for a complete period of vortex shedding were analyzed to explain the causes of lift force generation. Analysis of the effect of Reynolds numbers on the Strohal number was done. The analysis focused on the wake structure of the column at Re = 1000 and Re = 10000, and a significant difference was found between the two cases.

Key words: *finite-height cylinder, large eddy simulation, vortex structure*

Introduction

The flow around a cylinder has always been the focus of research in fluid mechanics. Most engineering problems can be studied from the flow around the cylinder, and the solutions can be applied in practice. In wind engineering, the air-flow around buildings has a significant impact on buildings. On one hand, buildings change the direction and structure of the original air-flow; on the other hand, the air-flow around the buildings generates drag force oscillations and lateral forces perpendicular to the direction of the air-flow, which directly affect the life and function of the buildings. Recently, the finite-height circular cylinder model (with one end fixed to the wall and the other end free) has been utilized for numerical studies because of its simplicity and representativeness. In contrast to the 2-D flow around the cylinder, the finite-length cylinder model has significant end effects, namely a fixed end and a free end, therefore, its flow field structure is much more complicated. Additionally, the finite-length cylinder model is more in line with the situation of real buildings (such as houses, launchers, chimneys, and high towers); therefore, research on the surrounding flow has a practical significance and value.

With the rapid development of CFD and rapid increase in computer speed and capacity, significant progress has been made in the theory and algorithm of high Reynolds numbers. Yuan [1] used the large eddy simulation (LES) method to perform a 2-D numerical simulation of the subcritical ($Re = 1.4 \cdot 10^5$) flow around an isolated cylinder. Wang *et al.* [2] performed 3-D numerical simulations (Re = 1000 and Re = 10000) of the flow around a fixed cylinder using the N-S equation without any turbulence model and reported that the flow around the cylinder at a high Reynolds number has distinct 3-D characteristics Breuer [3] performed a 3-D numerical simulation of the flow around an isolated cylinder (Re = 140000) using LES, and

* Corresponding author, e-mail: nieinhz@cjlu.edu.cn

the results revealed that 3-D numerical calculations of flow around a cylinder using the LES method agreed well with the experimental results. Pontaza and Chen [4] performed a 3-D numerical simulation of a two-degree-of-freedom cylindrical vortex-induced vibrations problem (Re = 100000) by using LES, and the numerical results conformed with those of Achenbach and Schewe.

Through a large number of literature surveys, it has been shown that many researchers worldwide have conducted in-depth and detailed research on the numerical simulation of 2-D flow around cylinders. For instance, Chen *et al.* [5] used the 2-D lattice Boltzmann method to predict the forces on a cylinder, as well as the frequency of vortex shedding. Cao *et al.* [6] numerically simulated the flow around a 2-D cylinder and demonstrated the flow characteristics as a function of Reynolds number. However, numerical studies on the 3-D characteristics of flow around a finite-height circular cylinder at medium and high Reynolds numbers are limited. Owing to the downwash effect on the upper-end face of the cylinder, the flow phenomenon around the cylinder is different from that of an infinitely long cylinder, and the 3-D characteristics are more significant [7]. Therefore, it is crucial to study this phenomenon. Given the aforementioned, this study adopted the LES method based on the turbulence model and used the CFD technology to simulate the flow field around a finite-height circular cylinder at a medium Reynolds number (Re = 1000-10000). The height-to-diameter ratio of the finite cylinder selected in this study was 8 (h/d = 8), and the Reynolds number was calculated using the diameter of the finite cylinder as the reference length; thus the final column lift and drag forces, Strouhal number, and column wake flow structure were calculated and analyzed.

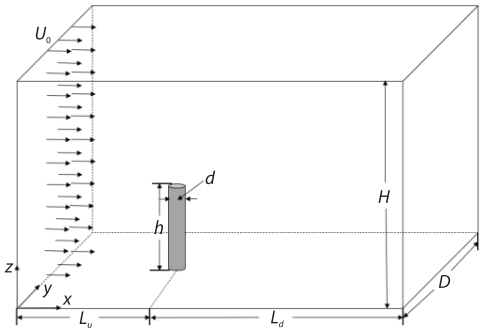

Figure 1. Model schematic

Problem description and numerical method

In this study, the turbulence model of a LES [1] was used for the numerical simulation, following a comprehensive literature review [8-10], we finally calculated the domain size and column placement, as shown in fig. 1, where the calculation domain size is $40d \times 30d \times 24d$, and to ensure that the wake flow can be fully developed, the finite-height circular cylinder in the calculation domain is $L_u = 12d$ from the entrance of the region and $L_d = 28d$ from the exit of the region. The diameter and height are d and h, respectively, and satisfy $h/d = 8$, and d is considered as 0.005 m in the calculation.

To solve the fluid equations of motion better, reasonable initial and boundary conditions must also be set. For the model shown in fig. 1, in this study, the inlet is set as the velocity inlet, and given uniform flow velocity U_0, the outlet is set as the pressure outlet, and its relative pressure is zero. The bottom and column surfaces were set as solid wall surfaces to satisfy the no-slip boundary condition ($u = v = w = 0$), and the front and back sides and top surface were set as symmetric surfaces; the following conditions were satisfied:

$$\frac{\partial u}{\partial y} = \frac{\partial w}{\partial y} = v = 0 \tag{1}$$

$$\frac{\partial u}{\partial z} = \frac{\partial v}{\partial z} = w = 0 \tag{2}$$

In the previous equation, u, v, and w denote the components of fluid velocity U in the direction of the co-ordinate axes x, y, and z, respectively.

In explicit calculations of n-dimensional problems, the time step should satisfy the Courant-Friedrichs-Lewy (CFL) condition [11], in this study, we take $n = 1$. The individual inlet fluid velocities U_0 were calculated according to different Reynolds numbers, and the corresponding time step t was calculated using CFL condition [11]. For example, when Re = 1000, the time step $t = 0.00025$ seconds is calculated to satisfy the condition.

The Strouhal number ($St = fd/U_0$) was used to describe the relationship between cylinder diameter, fluid velocity, and vortex shedding frequency, where f indicates the vortex shedding frequency, and Strouhal number can be obtained using FFT for the time history of the lift coefficient.

In this study, lift and drag coefficients were introduced to express the effect of flow on the column, and their expressions are:

$$C_l = \frac{F_l}{0.5\rho U_0^2 hd} \tag{3}$$

$$C_d = \frac{F_d}{0.5\rho U_0^2 hd} \tag{4}$$

where C_l and C_d denote the lift and drag coefficients, respectively, and F_l and F_d represent the forces on the column in the vertical flow direction and downstream direction, respectively, which are called the lift and drag forces on the column.

Furthermore, because the flow field structure of the finite-height circular cylinder is more turbulent at moderate Reynolds numbers and the amplitude of the lift coefficient fluctuates, the variable C_l' is introduced to represent the lift coefficient of the entire column, where C_l' is expressed by the root mean square value.

Validation

In this study, a structured grid was employed to mesh the entire flow field and the computational domain was divided into five regions. As depicted in fig. 2, this area of $1.5d \times 1.5d$ outside the cylinder is divided by an O-grid, and the grid of the cross area is increased. The first boundary-layer height was set around the cylinder to meet the requirement of $y^+ < 1$, and the other areas were divided by the H-grid. This allows the number of grids to be reduced, which is more conducive to the allocation of resources for computation and ensures the correctness of the LES method.

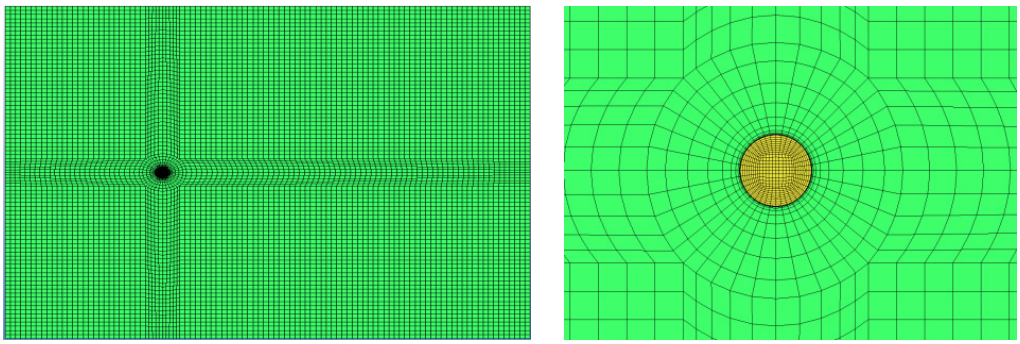

Figure 2. Schematic of the *x-y* plane mesh (a) and the 3-D *O*-shape of the flow area around a single-cylinder (b)

To verify the convergence and independence of the grid and verify whether the size of the grid has an impact on the calculation, three sets of grids were selected for analysis and comparison by dividing the calculation domain by the number of grids. The results are presented in tab. 1. Evidently, the Strouhal number values obtained from the three cases are very close, with a maximum error of approximately 1.5%. However, $\overline{C}_d$ deviates slightly, with the result of Case 2 being 8.5% larger than that of Case 1, whereas the result of Case 3 is approximately 5% larger than that of Case 2. The calculation results of Cases 2 and 3 are closer, with the errors being within the acceptable range, and both sets of meshes can be considered to have met the independence requirement. Considering computational efficiency, the grid setting of Case 2 was selected in this study.

Table 1. Mesh independence detection

Case	Number of grids	St	$\overline{C}_d$
1	1.2 million	0.1616	0.7859
2	2.34 million	0.1639	0.8589
3	3.94 million	0.1641	0.9034

To effectively verify the accuracy of the computational model, we selected Re = 3900, which was calculated by considering the diameter of the cylinder as the characteristic length. The results of the experiments and numerical simulations of previous studies were compared under the same Reynolds number and boundary conditions, as listed in tab. 2. Evidently, tab. 2 indicates that the Strouhal number results simulated in this study are nearly consistent with the experimental or simulation results obtained from previous studies. The maximum error with the numerical simulation is approximately 2.4%, and the error with the physical test is approximately 3%, which verifies the accuracy of the computational model in this study.

Table 2. Comparison of the simulated *St* results in this paper with those in the literature

	Methods	St	Error (with the results of this paper)
[12]	SST *k-w*	0.16611	1.3%
[13]	Physical tests	0.159	3%
[11]	LES	0.16	2.4%
Results of this paper	LES	0.1639	

Numerical results

In this study, the Reynolds number of is calculated for the finite-height cylinder simulation ranging from 1000-10000, and the results for Re = 1000 are initially examined. Graphs of the lift and drag coefficients obtained at Re = 1000 are shown in fig. 3(a). The figure shows that the lift coefficient C_l fluctuates around zero with an amplitude between –0.2 and 0.2, and the drag coefficient C_d fluctuates around one. To facilitate a comparison with previous literature results, the average drag coefficient C_d was calculated as 0.8973, and C_l was considered as the root mean square value to obtain C_l' as 0.0561. From fig. 3(a), it can also be observed that the system has been in stability fluctuations, and the observation of the C_l curve can be found to have a certain periodicity of fluctuations. The curve is analyzed by FFT spectrum to obtain fig. 3(b).

The Strouhal number value of the entire column was calculated to be 0.1418 after spectrum analysis. The aforementioned calculation results are compared with the results of the infinitely-high cylinder circulation experiment at Re = 1000 and listed in tab. 3. As shown in Tab. 3, all the results of this study have smaller values than those of the infinitely-high cylinder under similar boundary conditions. It is primarily because the flow around the cylinder of finite height is affected by the free end, and the free end will produce a *downwash* flow, which will gradually reduce the vortex shedding frequency of the Karman vortex street. The closer the free end is, the more visible the suppression effect, which even leads to the cylindrical surface vortex shedding on the vanishes, as elaborated in the following discussion.

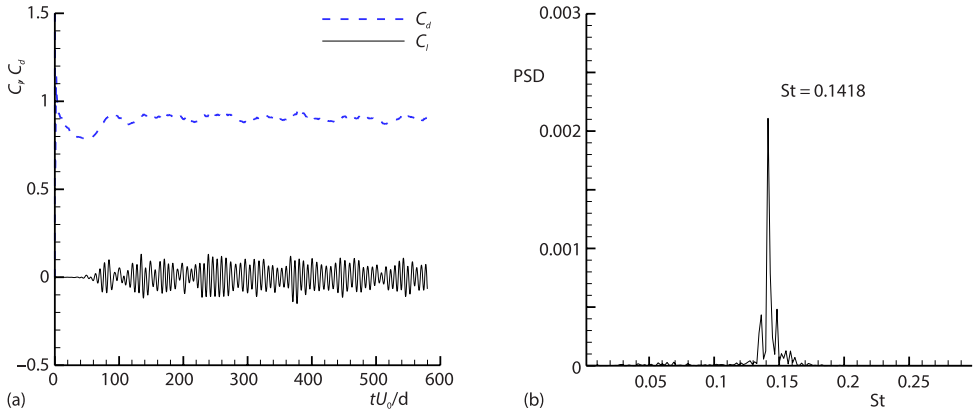

Figure 3. (a) Time history of drag and lift coefficients at Re = 1000 and (b) spectra corresponding to lift coefficients

Table 3. Comparison of flow around a finite and infinite cylinder when Re = 1000

Data source	$\bar{C}_d$	*St*
[14]	1.15	0.215
[15]	0.96	0.193
Results of this paper (LES)	0.8973	0.1418

Instantaneous contours of vorticity from different angles were selected for observation and analysis to verify the inhibition of vortex shedding at the column surface due to the *downwash* flow at the free end. Figures 4(a)-4(c) shows a vorticity diagram for different heights (z-direction). Figure 4(a) depicts the instantaneous contours of the vorticity at height $z = 7/8h$. It can be observed that there is no vortex shedding on the cylinder surface, indicating that the plane vortex shedding phenomenon at this height was almost completely suppressed, flow field situation was similar to the 2-D situation at a low Reynolds number, and two symmetrical re-circulation zones were formed behind the cylinder. Figure 4(b) shows the instantaneous contours of the vorticity at the middle height $z = 1/2h$. It can be seen that there is obvious vortex shedding on the column surface at this time, which indicates that the *downwash* flow at the free end does not act to the middle height, and these two figures can better illustrate the inhibition phenomenon at the free end. Figure 4(c) illustrates the instantaneous contours of the vorticity at height $z = 1/20h$. It can be observed in the fig. 4(c) that a horseshoe vortex is generated by the influence of the fixed end, which is caused by the non-slip property of the bottom surface.

Figure 4(d) shows the vorticity of the cross-sectional view of the computational domain. In the fig. 4, it can be observed that the vortex generated by the free end moves downward, suppressing vortex shedding on the cylindrical surface. It should be noted that the *downwash* inhibition phenomenon of the free end does not exist in the 2-D and 3-D infinite-height cylinders. Thus, the results of the flow around the finite-length cylinder in this study are smaller than those obtained by other infinite-length cylinders.

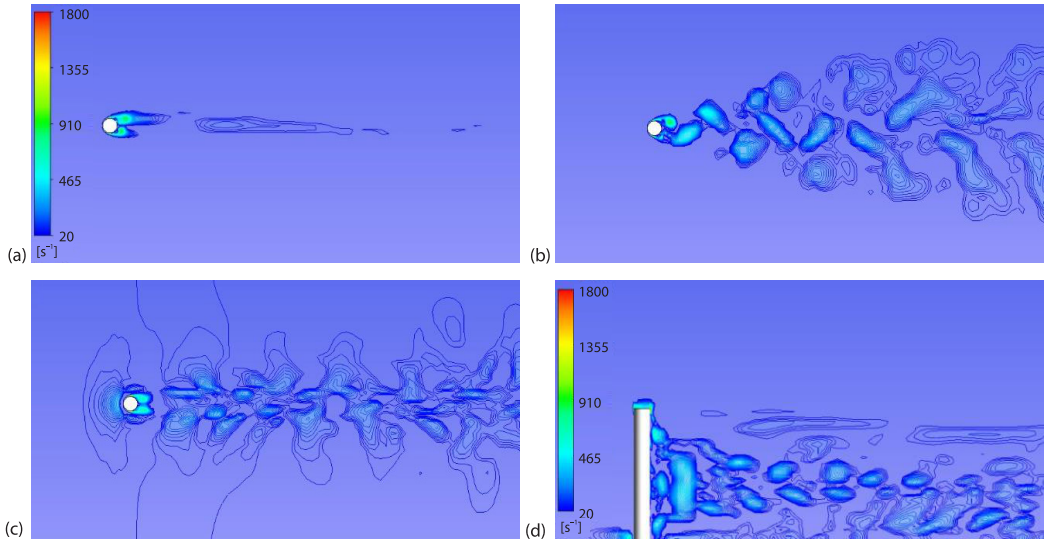

Figure 4. Instantaneous contours of vorticity at Re = 1000; (a) $z = 7h/8$, (b) $z = h/2$, (c) $z = h/20$, and (d) transverse vorticity, $y = D/2$

For the analysis of the wake flow structure of the column, four representative moments were selected: $t = 0$, $t = 1/4T$, $t = 1/2T$, $t = 3/4T$, T indicates the dimensionless period, and $T = 1/\mathrm{St}$ is defined. The top view ($z = 1/2h$) and sectional histogram ($y = D/2$) of the wake flow structure corresponding to the aforementioned four moments are shown in figs. 5 and 6, respectively. From the top view, it can be seen that when $t = 0$, the lower right side of the column produces a large vortex, fig. 7 shows the pressure diagram. This shows that the pressure at the center of the large vortex is the smallest, which is also one of the reasons for the generation of lift. The four moments shown in fig. 5 can be considered as the completion of a vortex shedding cycle, and the time spent in the shedding cycle corresponds to the shedding frequency and Strouhal number derived from the lift coefficient curve. Figure 6 illustrates a complete cycle of vortex shedding at the column surface in a direct view and the *downwash* flow at the free end, which also shows the horseshoe vortex generated at the fixed end and vortex street generated downstream, owing to the boundary-layer effect. In particular, fig. 8 depicts the 3-D vortex structure diagram of the finite-height cylinder corresponding to the aforementioned four moments to observe the complete vortex shedding process of the cylinder from a 3-D perspective. It can be seen that there are also staggered pairs of vortex structures in the wake flow field at Re = 1000, which can also be seen in the direct view in fig. 6, where pairs of vortex streets are generated downstream of the cylinder.

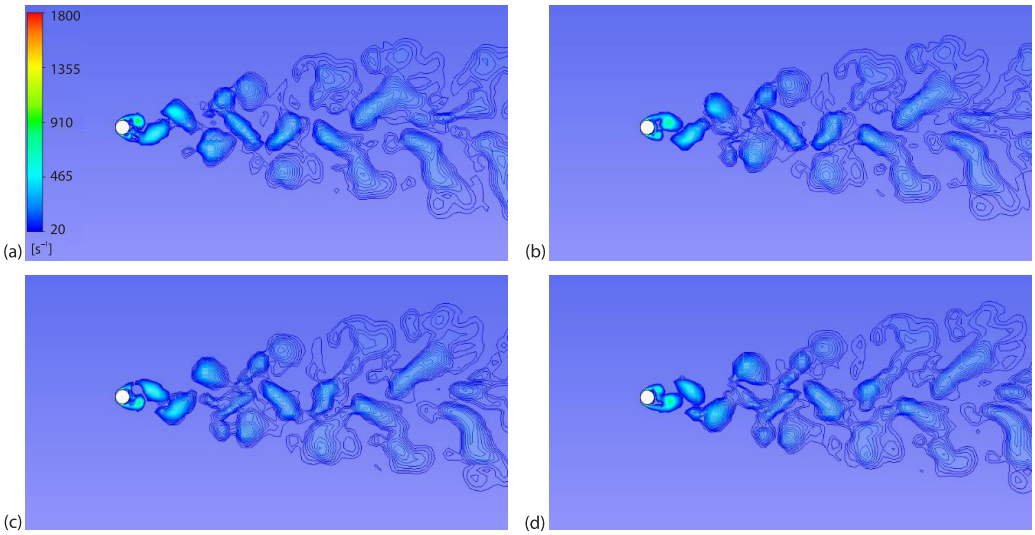

Figure 5. Instantaneous contours of vorticity during one period at Re = 1000 (top view); (a) $t = 0$, (b) $t = T/4$, (c) $t = T/2$, and (d) $t = 3T/4$

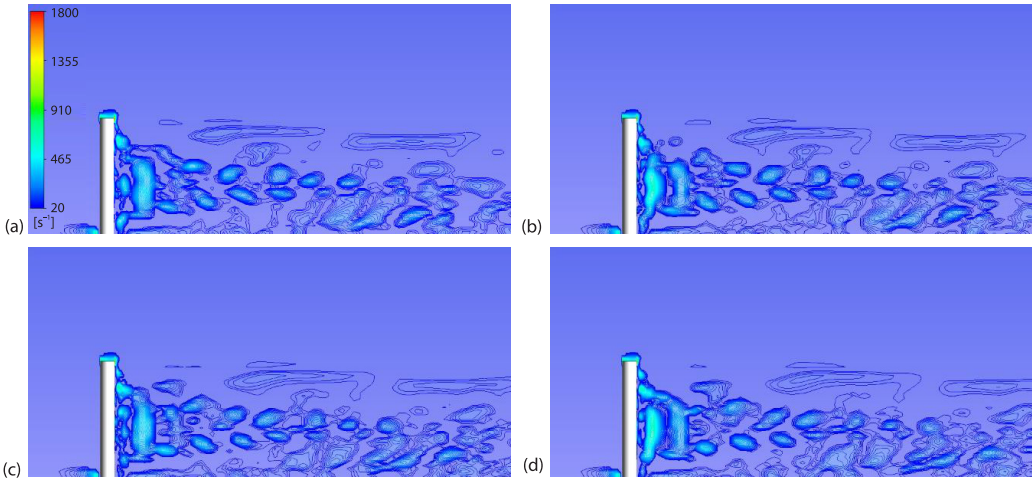

Figure 6. Instantaneous contours of vorticity during one period at Re = 1000 (front view); (a) $t = 0$, (b) $t = T/4$, (c) $t = T/2$, and (d) $t = 3T/4$

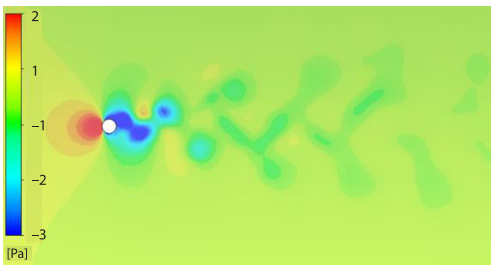

Figure 7. Instantaneous contours of pressure at Re = 1000 ($t = 0$)

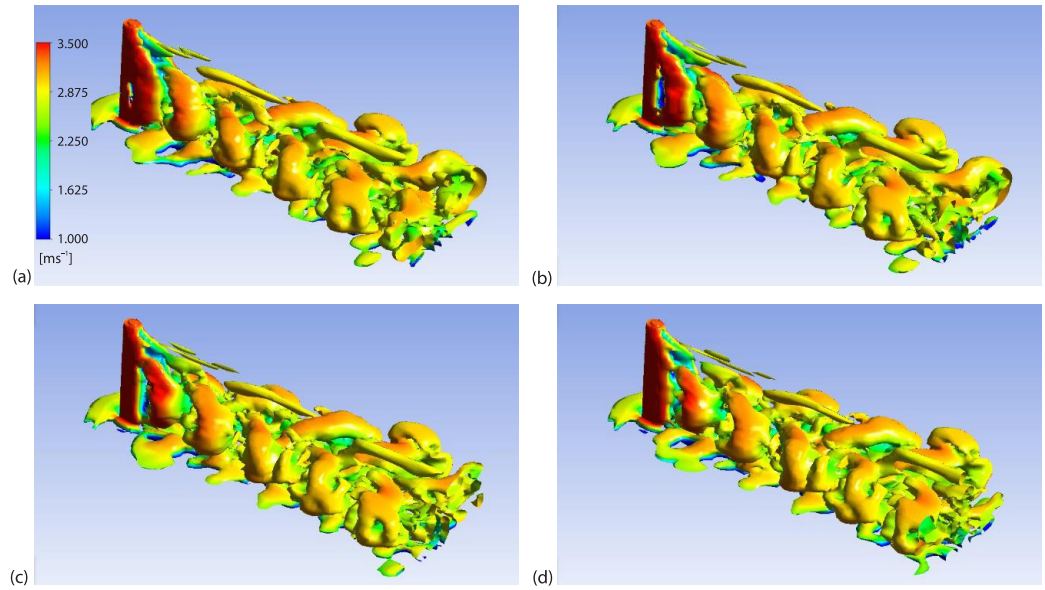

Figure 8. Iso-surfaces of instantaneous vortical structures colored with streamwise velocity during one period at Re = 1000; (a) $t = 0$, (b) $t = T/4$, (c) $t = T/2$, (d) $t = 3T/4$

Furthermore, the value of the Reynolds number started to increase, and the values of Strouhal number and C_l' at each Reynolds number were calculated to obtain fig. 9. It can be seen from the figure that as the Reynolds number increases, Strouhal number gradually increases at smaller Reynolds numbers (between Re = 1000-3000), and then tends to flatten out. Its value is almost constant, equivalent to a straight line.

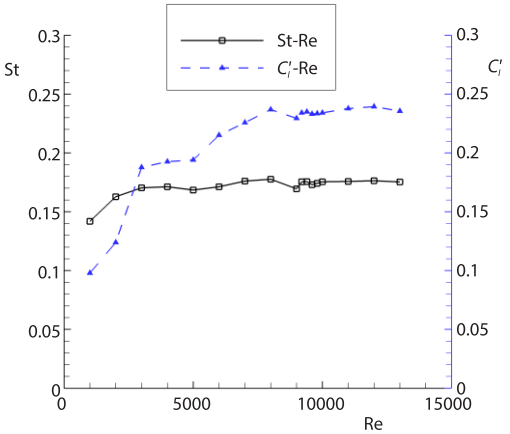

Figure 9. Dependence of Strouhal number on Reynolds number

Figure 9 also shows that the variation pattern of C_l' with Reynolds number is consistent with the variation pattern of Strouhal number with Reynolds number, primarily because the lift force described in this study is the combined force on the column in the vertical flow direction (y-direction), and the intensity of vortex shedding on the column surface is directly reflected in the magnitudes of C_l' and Strouhal number. Therefore, both can be used to describe the 3-D characteristics of the flow around a cylinder of finite height. As the difference in Strouhal number between Reynolds number between 6000 and 10000 is not large, and the 3-D vortex structure and wake flow are almost the same between them as observed in CFD simulation, this study examines the wake flow structure at Re = 10000 and compares it with the results at Re = 1000 to observe and analyze the differences in the wake flow between them.

The same method as that for Re = 1000 was adopted to examine and analyze the wake flow structure of the column at Re = 10000. A complete vortex shedding period was selected

from the lift coefficient curve after reaching a steady-state, and four representative moments were selected, corresponding to $t = 0$, $t = T/4$, $t = T/2$, and $t = 3T/4$, respectively.

Figures 10 and 11 illustrate the distribution of vorticity in the top view ($z = h/2$) and profile histogram ($y = D/2$) for the four representative moments mentioned previously. It can also be seen from the top view of a complete cycle that multiple vortices of different scales are shed on one side of the tail of the cylinder at each instant and subsequently move toward the centerline. The process of vortex generation and shedding is not the same each time, and there is a certain randomness, which is not observed when Re = 1000. Additionally, the top view shows

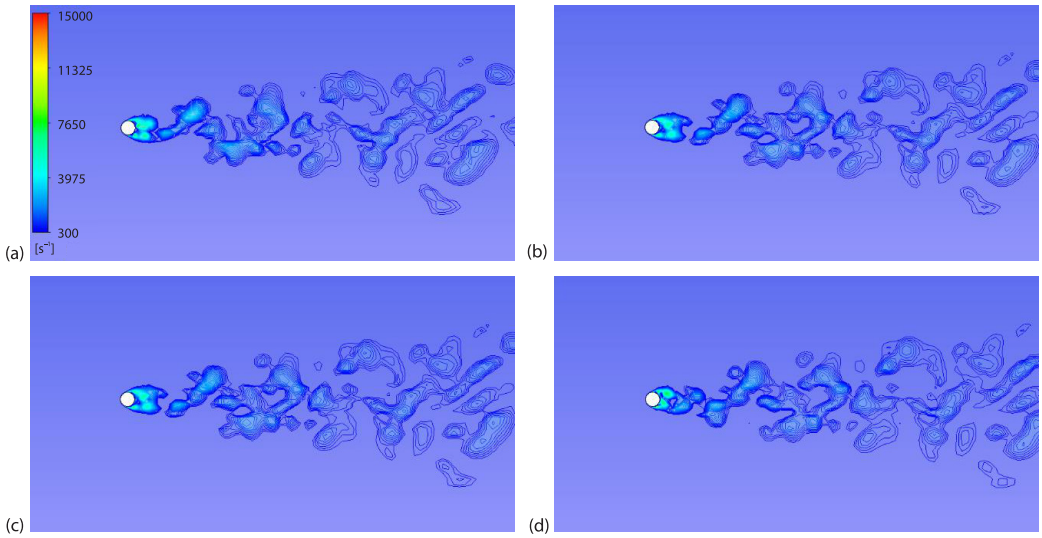

Figure 10. Instantaneous contours of vorticity during one period at Re = 10000 (top view); (a) $t = 0$, (b) $t = T/4$, (c) $t = T/2$, and (d) $t = 3T/4$

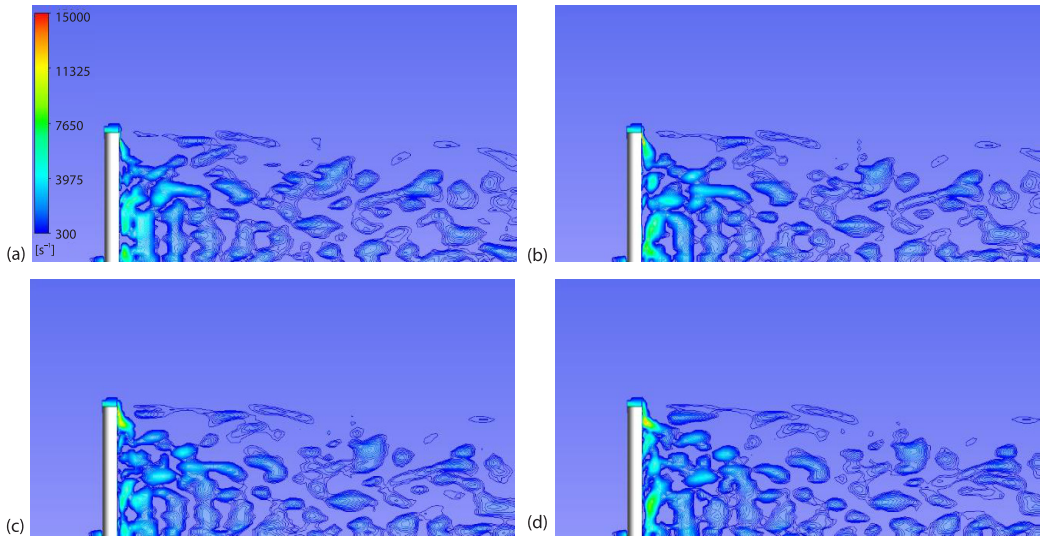

Figure 11. Instantaneous contours of vorticity during one period at Re = 10000 (front view); (a) $t = 0$, (b) $t = T/4$, (c) $t = T/2$, and (d) $t = 3T/4$

that the downstream of the column has become more turbulent, and the vortex off the column has become asymmetrical, as shown in the fig. 10. Therefore, it is no longer the standard Carmen vortex distribution, indicating that the *downwash* flow at the free end has influenced the development of the vortex off the column surface in the middle, which is one of the differences between Re = 10000 and Re = 1000. The front view in fig. 11 confirms this statement. It can be observed that the downwash flow at the free end has almost affected the middle height of the column, however, it can also be seen from the front view that the vortex shedding can still be seen in the height of the column from the bottom to the middle part of the column, which shows that the downwash has not completely disturbed the flow field of the whole column, from the bottom to half of the height of the column, the main part of the flow is still Carmen vortex street.

Observing the vorticity distribution of the profile diagram for both in figs. 6(a) and 11(c) when Re = 1000 and 10000, respectively, it is obvious that the vorticity value at Re = 10000 is much larger than that at Re = 1000, and there are still vortex streets formed downstream of the cylindrical column at Re = 1000, while the flow downstream of the column has become sufficiently turbulent when Reynolds number reaches 10000 that there is no longer any obvious vortex street generated. Figure 12 illustrates the 3-D vortex structure of Re = 1000 can also be seen in the vertical and horizontal vortex, while Re = 10000 no longer has this phenomenon, the flow field has become extremely turbulent, which also conforms with the characteristics of large Reynolds number turbulence. It should be mentioned that figs. 6(a), 11(c), and 12 are plots made at the moment when their lift curves reach their maximum, primarily to ensure that they are comparable.

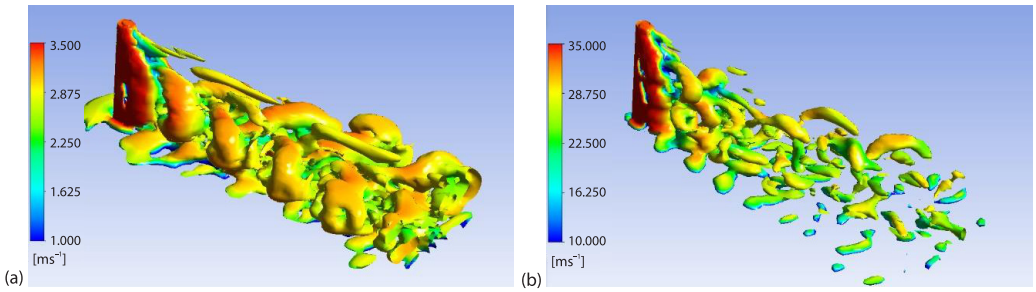

Figure 12. Iso-surfaces of instantaneous vortical structures colored with streamwise velocity; (a) Re = 1000 and (b) Re = 10000

Conclusion

In this study, based on LES method, the flow problem around a cylinder of finite height was examined. By comparison with the results in the literature, the accuracy of the simulation method in this study was confirmed. Between Re = 1000-10000, the forces on the column and the wake flow characteristics were examined and analyzed, and the following conclusions were drawn.

- Unlike the infinite-height cylinder, the finite-height cylinder has a weakened wake flow owing to the destruction of the original Carmen vortex flow pattern caused by the downwash flow at the free end, making its average drag coefficients C_d, Strouhal number, and C_l' (lift coefficients considered as root-mean-square values) lower than those of the infinite-height cylinder. Additionally, it is evident from the pressure diagram that the pressure at the center of the large vortex is the smallest when the vortex on the cylindrical surface begins to fall off, which is one of the principal reasons for the generation of the

lift. At the bottom of the cylinder, the presence of solid walls led to a typical horseshoe vortex at the front end of the bottom of the cylinder. This vortex also has some effect on the flow downstream of the column, however, it is smaller compared with the effect produced at the end.

- When the Reynolds number was small (Re = 1000), pairs of vortices were generated downstream of the column, and the flow was dominated by the Carmen vortex. In the top view, it can be seen that the column exhibits a 2P pattern of vortex shedding in the middle, *i.e.*, two pairs of vortices are generated per cycle, and each pair consists of two vortices in opposite directions. In a 3-D vortex structure, the vortices are staggered in pairs. By gradually increasing the Reynolds number in the range of 1000-10000, the value of Strouhal number increases with the increase in Reynolds number, the downstream flow of the column starts to become turbulent, downwash effect of the free end is enhanced, and the change in Strouhal number tends to be a straight line. Additionally, the variation pattern of C_l' remained nearly the same as that of Strouhal number, indicating that both can qualitatively describe the variation in the lift of the column.
- When Re = 1000, the downstream of the column becomes sufficiently turbulent after Reynolds number reaches 10000, the downwash flow at the free end affects the plane where the middle height of the column is located, and there are no longer pairs of staggered vortices downstream of the column. Multiple vortices are shed on the side of the column tail at each instant, and each vortex has a different scale, subsequently moving toward the centerline. Each vortex generation and shedding process is not the same, and there is a certain degree of randomness.

Acknowledgment

This study was supported by the National Natural Science Foundation of China (No.12132015 and No.11972336).

References

[1] Yuan, M. S., High Reynolds Number Flow Around a Cylinder of 2-D Large Eddy Simulation (in Chinese), *Water Dynamics Research and Development*, *7* (1992), Suppl., pp. S614-S622
[2] Wang Y. L., *et al*., The 3-D Numerical Simulation of Viscous Flow Around Circular Cylinder (in Chinese), *Journal of Shanghai Jiao Tong University*, *35* (2001), 10, pp. 118-122
[3] Michael B., A Challenging Test Case for Large Eddy Simulation: High Reynolds Number Circular Cylinder Flow, *International Journal of Heat and Fluid-Flow*, *21* (2000), 5, pp. 648-654
[4] Pontaza J., Chen H., The 3-D Numerical Simulations of Circular Cylinders Undergoing Two Degree-of-Freedom Vortex-Induced Vibrations, *Journal of Offshore Mechanics and Arctic Engineering*, *129* (2007), 3, pp. 158-164
[5] Chen Y., *et al.*, Numerical Simulation of Flow Around a Circular Cylinder at Different Reynolds Numbers (in Chinese), *China Water Transport, 15* (2015), 7, pp. 88-90
[6] Cao G. L., *et al.*, Numerical Simulation of the Flow of a 2-D Incompressible Viscous Fluid Around a Blunt Body (in Chinese), *Gansu Science and Techmology, 28* (2012), 8, pp. 57-59
[7] Sumner, D., Flow Above the Free end of a Surface-mounted Finite-Height Circular Cylinder: A Review, *Journal of Fluids and Structures, 43* (2013), Nov., pp. 41-63
[8] Burger M., *et al.*, The DNS of Droplet-Vortex Interaction with a Karman Vortex Street, *International journal of heat and fluid-flow, 27* (2006), 2, pp. 181-191
[9] Catalano P., *et al*., Numerical Simulation of the Flow Around a Circular Cylinder at High Reynolds Numbers, *International Journal of Heat and Fluid-Flow*, *24* (2003), 4, pp. 463-469
[10] Dong, S., Karniadakis, G., The DNS of Flow Past a Stationary and Oscillating Cylinder at Re = 10000, *Journal of Fluids and Structures*, *20* (2005), 4, pp. 519-531
[11] Wang X. C., *et al*., Numerical Simulation of 3-D Flow Around a Circular Cylinder of Finite Length (in Chinese), *Chinese Journal of Ship Research*, *13* (2018), 2, pp. 27-34

[12] Gao, Journal Numerical Study on Free End Effect of Flow around a Cylinder (in Chinese), M. Sc. thesis, Harbin Engineering University, Harbin, China, 2019
[13] Park, C., Lee, S., Free end Effects on the Near Wake Flow Structure Behind a Finite Circular Cylinder *Journal of Wind Engineering and Industrial Aerodynamics*, *88* (2000), 2, pp. 231-246
[14] Braza, M., *et al.*, Numerical Study and Physical Analysis of the Pressure and Velocity Fields in the Near Wake of a Circular Cylinder, Journal of Fluid Mechanics, *165* (1986), Apr., pp. 79-130
[15] Wanderley J., *et al*., Vortex-Induced Vibration of an Elastically Mounted Circular Cylinder Using an Upwind TVD 2-D Numerical Scheme, *Ocean Engineering*, *35* (2008), 14-15, pp. 1533-1544

Paper submitted: March 12, 2022
Paper revised: March 24, 2022
Paper accepted: April 14, 2022